

Comparison of LMI Solvers for Robust Control of a DC-DC Boost Converter

^{1,*} Jérôme BOSCHE, ² David LARA ALABAZARES
and ¹ Abdelhamid RABHI

¹ Modeling, Information and Systems, UPJV, 33 rue Saint-Leu, 80000, Amiens, France

² Instituto Tecnológico Superior de Misantla, Carretera a Loma del Cojolite,
93821 Misantla, Veracruz, México

¹ Tel.: + 33322825915, fax: + 33322825905

* E-mail: jerome.bosche@u-picardie.fr

Received: 17 April 2023 Accepted: 19 May 2023 Published: 26 June 2023

Abstract: This work deals with a robust Fault-Tolerant Control (FTC) design for a class of uncertain systems. Fault resilience is associated with a robustness bound generated by a sufficient Linear Matrix Inequality (LMI) condition for static state feedback stabilization. This design control approach is based on solving an optimization problem expressed in terms of LMI with three different programming solvers which are *mincx* (MATLAB), *lmsolver* (SCILAB) and *cvxopt* (PYTHON). Numerical validations were carried out, first on an academic model, then on the model of a PV energy conversion system connected to a DC-DC boost converter. Then, a robustness analysis for fault resilience associated with a control law gains, obtained using the three solvers, was realized to investigate the best performance. This approach was finally validated on an experimental test bench.

Keywords: Fault, Tolerant control, Robust state feedback control, LMI, DC/DC boost converter, MATLAB, SCILAB, PYTHON.

1. Introduction

Cyber-physical Systems (CBS) are increasingly complex and sophisticated. The challenge is to exploit new technologies and hardware to make them more efficient and autonomous [1]. Sensors are associated with CBS to get precise environment information, allowing the system to be autonomous, as much as possible. However, this poses two major problems: (a) how to make the system react effectively based on real-time sensor data? (b) how to take into account a fault sensor during operation? Fault Tolerant Control (FTC) studied in the field of control theory, can solve this problem. It is applied as a tool in transport [2], energy [3], industry 4.0 [4], etc. In the case of a partial fault, the FTC problem can be formulated as a state

feedback control (SFC) problem for an uncertain system with a norm-bounded uncertainty. Then, a controller guaranteeing a certain level of performance for the largest uncertainty domain is designed. When the fault is total, a SFC augmented with an observer or outright, an output feedback control (OFC) law, are suitable. Finally, it is possible to consider the general case of partial and/or total faults by using a robust OFC. Concerning partial fault, the approach of [5] can be exploited to design an FTC. In this work, a α -stabilization technique is used to compute a passive fault-tolerant control law that guarantees the asymptotic stability of the system in the presence of faults.

On the other hand, the pole placement of the closed-loop system in a region α of the complex

plane, allows the process to react efficiently to the fault. Whatever the technique, it must lead to a control law as robust as possible, the capacity of the system to tolerate the fault depending on this robustness. In fact, most of the work relating to this issue tends to reduce the conservatism induced by the sufficient conditions, related to a LMI problem, and leading to the gain of the controller. Some LMI-based conditions consider non-quadratic Lyapunov functions [6], other works rather exploit homogeneous polynomial Lyapunov functions [7] while promising results are obtained with fuzzy Lyapunov functions [8]. Then, significant advances have been made in this area, but these new conditions, less conservative, consist in LMI systems that are increasingly complex to solve from a numerical point of view. However, it is interesting to note that the robustness of these control laws may depend on the numerical computation software used to solve the problem, and more globally, on the associated LMI solver. Solving an LMI amounts to a semidefinite programming problem (SDP). There are many algorithms for solving SDP and many of them use the interior-point method [9]. Interior point algorithms are often combined with second-order optimization methods using Newton's method. They are particularly efficient for small SDP. For more complex problems, first-order optimization methods using the gradient descent method are more suitable. In [10], an efficient randomized first-order algorithm for solving SDP is proposed and compared to the CVXOPT solver of PYTHON [11] and the Splitting Conic Solver algorithm [12]. This work considers rather small-dimensional SDP and we will solve our LMI problems using PYTHON's CVXOPT solver [11], SCILAB's LMISOLVER solver [13] and MATLAB's MINCX solver [14]. The robustness of a control law associated with a DC-DC boost converter is then analyzed according to the solver used.

The paper is organized as follows: Section 2 is dedicated to some preliminaries which present the uncertainty models considered in this work as well as the concept of robust α - stabilization. Section 3 deals with the modeling of the DC-DC boost converter considering sensor faults and the control objectives. Section 4 compares the efficiency of the three LMI solvers. Initially, the α - stabilization of a numerical model is considered, then the problem of the voltage regulation of a PV module is dealt with. Section 5 presents an experimental validation of the FTC control approach on photovoltaic energy conversion chain while section 6 gives conclusions and perspectives.

2. Preliminaries

We denote by M^T , the transpose of M . \mathbb{I}_n is the identity matrix of order n . \mathbb{O} is a null matrix of suitable dimension. $\{\blacksquare\}^T$ standing block (i,j) in a matrix corresponds to the transposed term of block (j,i). $\Gamma(A)$ is the spectrum of the matrix A , that is to

say, the set of its eigenvalues. \mathcal{C} is the complex plane and \mathcal{C}^- stands for $Re(\mathcal{C}) < 0$.

2.1. Polytopic and Norm-Bounded Representation

The Polytopic and Norm-Bounded (PNB) representation is used to robust analysis and control dedicated to systems affected by both polytopic and structured uncertainties, represented in the state space by the following model:

$$\begin{cases} \dot{x}(t) = A(\theta).x(t) + B(\theta).u(t) + T.\varphi(t). & (1) \\ y(t) = C(\Delta).x(t), & (2) \end{cases}$$

where $x(t) \in \mathbb{R}^n$, $u(t) \in \mathbb{R}^m$, $y(t) \in \mathbb{R}^p$, and $\varphi(t) \in \mathbb{R}^v$ are respectively the state, input, output and measurable disturbance vectors. $A(\theta) \in \mathbb{R}^{n \times n}$ and $B(\theta) \in \mathbb{R}^{n \times m}$ represent the state and control matrices, belonging to a polytopic of matrices with N vertices:

$$[A(\theta)B(\theta)] = \sum_{i=1}^N \theta_i [A_i B_i] \quad (3)$$

$$\text{with } \sum_{i=1}^N \theta_i = 1. \quad (4)$$

$C(\Delta)$ is the output matrix affected by a norm-bounded uncertainty, denoted \mathcal{JL} -structured uncertainty, whose representation is recalled here:

$$C(\Delta) = C_0 + \mathbb{E} = C_0 + J.\Delta.L, \quad (5)$$

where C_0 is a nominal matrix, $J \in \mathbb{R}^{n \times q}$ and $L \in \mathbb{R}^{r \times n}$ are known structured matrices whereas $\Delta \in \mathbb{R}^{q \times r}$ is the uncertain matrix belonging to the ball $\mathcal{B}(\rho)$ such that $\|\Delta\|_2 < \rho$. \mathbb{E} is a norm-bounded uncertainty whose structure is defined par J and L .

2.2. α -stabilization

This part addresses the design of robust feedback control for a system with PNB uncertainties and particular attention is paid to the system dynamic performance, such as the time response. Also, the placement of all spectrum of the state-matrix $\Gamma(A_C = A(\theta) + B(\theta).K)$ in a half plane \mathcal{C}^α of \mathcal{C}^- is treated, defined by $x < \alpha$. Then, when $(A_C) \in \mathcal{C}^\alpha$, A_C is said α -stable.

A sufficient condition of robust α -stabilization by static state feedback deduced from that proposed by [5] is recalled here. Therefore, it does not constitute an original contribution in the context of this work but rather a robust control law technique which will be processed by different solvers and analyzed.

Theorem 1. There is a matrix K associated with the robust state control law $u(t) = K.x(t)$ α -stabilizing system (1)-(2), if there is a solution to the following convex optimization problem

$$\min_{X, R, \zeta} \gamma = \rho^{-2}, \quad (6)$$

where ζ is a positive scalar fixed a priori, $X = X^T > 0$, $X \in R^{n \times n}$, $R \in R^{m \times n}$ and γ are variables verifying the LMI constraints:

$$H_i(A_i, B_i, J_i, L_i, T) < 0, \quad \forall i \in \{1, \dots, N\} \quad (7)$$

with

$$H_i = \begin{bmatrix} Q_i & \{\blacksquare\}^T & \{\blacksquare\}^T & \{\blacksquare\}^T & \{\blacksquare\}^T \\ L_i X & -\mathbb{I}_r & \mathbb{O} & \mathbb{O} & \mathbb{O} \\ X & \mathbb{O} & -\mathbb{I}_n & \mathbb{O} & \mathbb{O} \\ J_i^T & \mathbb{O} & \mathbb{O} & -\gamma \mathbb{I}_q & \mathbb{O} \\ T^T & \mathbb{O} & \mathbb{O} & \mathbb{O} & -\zeta \mathbb{I}_v \end{bmatrix}$$

with $Q_i = \{-\alpha X + A_i X + B_i R\} + \{\blacksquare\}^T$

A static state feedback is then associated with:

$$K = R \cdot X^{-1} \quad (8)$$

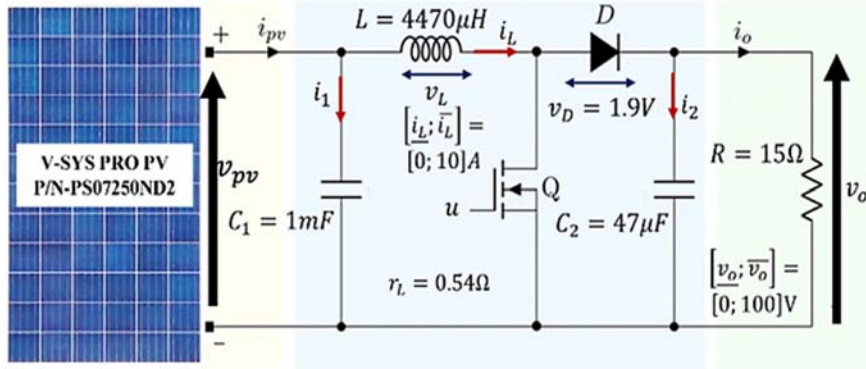


Fig. 1. DC-DC boost converter for a PV module

3.1. PNB Representation of a Boost Converter

The averaged model of this system considers two sub-models: one is associated with an “off state” of the thyristor ($u(t)=0$), the other with an “on state” ($u(t)=1$). It can be written in the form (1) with $x(t) = [i_L(t) v_0(t) v_{PV}(t)]^T$, $\varphi(t) = [v_D \quad i_{PV}(t)]^T$ where $i_L(t)$ is the inductor current, $v_0(t)$ is the output voltage, and $v_{PV}(t)$ the PV voltage generated by the module. Basically, the dynamic equations of the boost converter can be expressed by the Linear Parameter-Varying (LPV) state-space equation (1) with:

$$A = \begin{bmatrix} -\frac{r_L}{L} & \frac{(u_0 - 1)}{L} & \frac{1}{L} \\ \frac{(1 - u_0)}{C_2} & -\frac{1}{RC_2} & 0 \\ -\frac{1}{C_1} & 0 & 0 \end{bmatrix} \quad (9)$$

and the uncertainty domain for which the α -stability is guaranteed is given by $\|\Delta\|_2 \leq \rho^* = \gamma^{-\frac{1}{2}}$, the optimal value of ρ .

3. FTC for DC-DC Boost Converter

The DC-DC boost converter system, associated with a photovoltaic module, connected to a load is shown in Fig. 1. It fits into our problem and will be used to support a comparison of the fault resilience resulting from the resolutions of control optimization problems.

The converter consists of: a) a power transistor Q and a rectifier diode D (threshold voltage v_D) constituting the switching-mode power device, b) a smoothing inductance L with internal resistance r_L , and c) a filtering voltage capacity C_1 and a bus capacity C_2 .

$$B(\theta(t)) = \begin{bmatrix} (v_0(t) + v_D) \\ \frac{L}{-i_L(t)} \\ \frac{C_2}{0} \end{bmatrix} \quad (10)$$

$$T = \begin{bmatrix} (u_0 - 1) & 0 \\ \frac{L}{0} & 0 \\ 0 & \frac{1}{C_1} \end{bmatrix} \quad (11)$$

Note that the control matrix $B(\theta(t))$ depends on time-varying states $i_L(t)$ and $v_0(t)$, leading to a nonlinear the model. Nevertheless, the range of signal variation is bounded, as shown in Fig. 1, so $B(i_L(t), v_0(t))$ can be considered as a polytope of matrices as in (3) with $N=4$, $B_1 = B(\bar{i}_L, \bar{v}_0)$, $B_2 = B(\bar{i}_L, v_0)$, $B_3 = B(i_L, \bar{v}_0)$ and $B_4 = B(i_L, v_0)$.

On the other hand, under normal operating conditions, the states are measured by current and

voltage sensors, respectively noted S_{I_L} , S_{v_0} and $S_{v_{PV}}$. Then, it is assumed that these sensors can be affected by a fault. Depending on the value of $C(\Delta)$ in (5), three cases are considered associated with $C_0 = \mathbb{I}_3$ and the corresponding values for J and L , as shown Table 1.

Table 1. Three fault cases for the DC-DC boost converter.

Case	J	L	S_{I_L}	S_{v_0}	$S_{v_{PV}}$
1	$B(\theta)$	[1,0,0]	partial	none	none
2	$B(\theta)$	[0,1,0]	none	partial	none
3	$B(\theta)$	[0,0,1]	none	none	partial

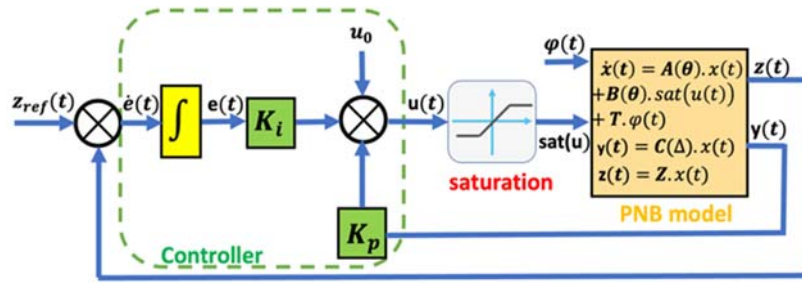


Fig. 2. nPI controller architecture.

The input command is saturated, $u(t) \in [\bar{u}; \underline{u}]$, with $\bar{u} = u_0 - \delta_u(t)$ and $\underline{u} = u_0 + \delta_u(t)$, where u_0 is the nominal value of $u(t)$. In order to take into account the integral action inherent in this control architecture, the state-space representation (1)-(2) is extended to an augmented model with a state vector resulting from the concatenation of $x(t)$ and $e(t)$, the integral of the error between the reference signal $z_{ref}(t)$ and $z(t)$, the signals to be regulated. Without difficulty, we obtain the corresponding representation.

$$\begin{cases} \dot{X}(t) = \mathbb{A}.X(t) + \mathbb{B}.u(t) + \mathbb{T}.\varphi(t) + \mathbb{F}.z_{ref}(t) & (14) \\ y(t) = \mathbb{C}(\Delta).X(t) & (15) \end{cases}$$

with

$$\begin{cases} X(t) = \begin{bmatrix} x(t) \\ e(t) \end{bmatrix}, \mathbb{A} = \begin{bmatrix} A(\theta) & \mathbb{O} \\ -Z & \mathbb{O} \end{bmatrix}, \mathbb{B} = \begin{bmatrix} B(\theta) \\ \mathbb{O} \end{bmatrix} \\ \mathbb{T} = \begin{bmatrix} T \\ \mathbb{O} \end{bmatrix}, \mathbb{F} = \begin{bmatrix} \mathbb{O} & \mathbb{O} \\ \mathbb{O} & \mathbb{I}_z \end{bmatrix}, \mathbb{C}(\Delta) = \begin{bmatrix} C(\Delta) & \mathbb{O} \\ \mathbb{O} & \mathbb{I}_z \end{bmatrix} \end{cases} \quad (16)$$

3.3. FTC Controller of a Boost Converter

According to part 3.2, it is clear that $z_{ref}(t) = v_{PVref}(t)$ and $z(t) = v_{PV}(t)$. It leads to

3.2. Control Objective

Our control objective is to exploit the α -stabilization condition to develop a proportional-integral regulator, whose architecture is shown in Fig. 2.

$z(t) \in \mathbb{R}^z$ is the controlled output vector and the problem consists in regulating $z(t)$ to a reference value $z_{ref}(t)$. The control law results in n proportional actions (one for each state variable) and one integral action (on the error). The corresponding n PI controller is then defined by:

$$u(t) = u_0 + K_p.y(t) + K_i.e(t) = u_0 + \delta u(t). \quad (12)$$

$$\text{with } e(t) = \int_0^t (z_{ref}(\tau) - z(\tau)).d\tau \quad (13)$$

$E = [0 \ 0 \ 1]$ and then, the augmented DC-DC boost converter model is easily deduced from (14), (15), (16) with (9), (10) and (11). A fault-tolerant control law can then be computed if there is a solution to the convex optimization problem (6) verifying LMI conditions:

$$H_i(\mathbb{A}_i, \mathbb{B}_i, \mathbb{J}_i, \mathbb{L}_i, \mathbb{T}) < 0, \quad \forall i \in \{1, \dots, 4\} \quad (17)$$

$$\begin{bmatrix} \mu_1 \mathbb{I}_n & R^T \\ R & \mathbb{I}_m \end{bmatrix} > 0 \quad (18)$$

$$\begin{bmatrix} \mu_2 \mathbb{I}_n & \mathbb{I}_n \\ \mathbb{I}_n & X \end{bmatrix} > 0 \quad (19)$$

where $\mathbb{J}_i = [J_i \ \mathbb{O}]^T$ and $\mathbb{L}_i = [L_i \ \mathbb{O}]$ and LMIs (18) and (19) respectively limit the 2-norm of R and X^{-1} , and consequently the controller gain values.

4. Simulation Results

This section is dedicated to simulation results. First, the robust α -stabilization is applied on a numerical model and generated by the three LMI solvers. Subsequently, this same stabilization technique is tested on the photovoltaic energy conversion system presented in Section 3, as in [9].

4.1. Numerical Model Simulations

We consider the polytopic and norm-bounded representation of a numerical model described below:

$$A_1 = \begin{bmatrix} -2 & -1 & 0 \\ 0 & 10 & 1 \\ 0 & 0 & -1 \end{bmatrix} \text{ and } A_2 = \begin{bmatrix} -2 & -1 & 0 \\ 2 & 10 & 1 \\ 0 & 0 & -1 \end{bmatrix}$$

$$B_1 = B_2 = \begin{bmatrix} 2 \\ -1 \\ 1 \end{bmatrix} \text{ and } J_1 = J_2 = B_1 = B_2$$

Then three fault sensor cases are considered:

- Case 1:** 1st sensor fault with $L_1 = L_2 = [1 \ 0 \ 0]$;
Case 2: 2nd sensor fault with $L_1 = L_2 = [0 \ 1 \ 0]$;
Case 3: 3rd sensor fault with $L_1 = L_2 = [0 \ 0 \ 1]$.

Then, the optimization problem (6) considering LMI conditions (7) with $T = \mathbb{O}$ (no disturbance) has been solved using the MATLAB's *mincx* function, the SCILAB's *lmisolver* function and the PYTHON's *cvxopt* function for the three fault sensor cases and for $\alpha = -1, -2, -3$ and -5 . Table 2 shows the robustness bound values obtained for each case. When no value is provided, it means that the LMI system could not be solved by the corresponding solver. Colored cells correspond to the highest bound.

These results show that SCILAB's *lmisolver* leads each time to the best robustness bound, that is to say to the best sensor fault tolerance. However, note that the results obtained with this solver are very close to those obtained with *mincx* from MATLAB. PYTHON's *cvxopt* function seems, in this case, to offer less robustness.

4.2. DC-DC Boost Converter Simulations

It is about computing the nPI controller presented in part 3.2 to regulate the photovoltaic voltage of a PV module. The control objective is to generate the duty

cycle of signal $u(t)$ for the gate of Q to regulate the voltage $v_{pv}(t)$ to the reference photovoltaic voltage $v_{pvref}(t)$. An MPPT algorithm (not detailed in this work) generates the reference PV voltage from data (weather, current, voltage) acquired on an experimental set-up. The architecture of this implementation is shown in Fig. 3.

Table 2. Robustness bounds ρ^* .

Case	α	LANGUAGE		
		MATLAB	SCILAB	PYTHON
1	-1	5.0641	5.0777	4.9808
	-2	5.0439	5.0547	4.6120
	-3	4.8956	4.9068	2.5509
	-5	---	---	---
2	-1	5.0631	5.0776	4.9766
	-2	5.0424	5.0562	4.6451
	-3	4.9288	4.9328	3.0610
	-5	2.9135	2.9217	---
3	-1	5.0635	5.0774	4.9583
	-2	5.0420	5.0560	4.6212
	-3	4.9240	4.9299	2.8493
	-5	2.6839	2.6896	---

For this simulation, it is supposed that the corresponding $v_{pvref}(t)$ is computed over a 12 hours period starting at 7:00 am, as showed Fig. 4, with the PV current $i_{pv}(t)$ generated by the panel shown at Fig. 5.

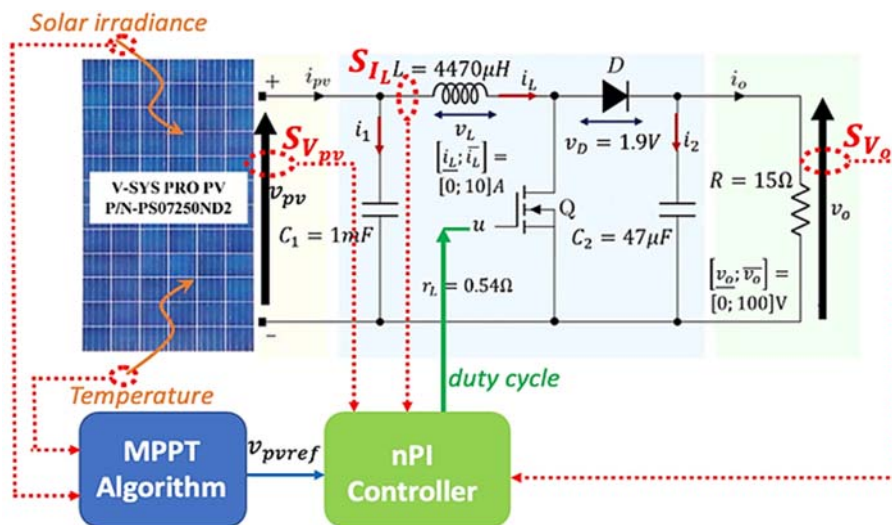


Fig. 3. Controller implementation.

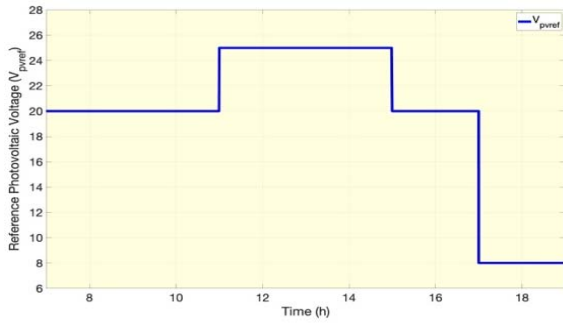


Fig. 4. Reference Photovoltaic voltage $v_{PVref}(t)$.

The Fault-Tolerant Control technique presented in the Section 3.3 has been tested on the DC-DC boost converter of Section 3.1. Once again, three fault sensor cases are considered:

Case 1: i_L sensor fault with $L_1 = L_2 = [1 \ 0 \ 0]$;

Case 2: v_o sensor fault with $L_1 = L_2 = [0 \ 1 \ 0]$;

Case 3: v_{pv} sensor fault with $L_1 = L_2 = [0 \ 0 \ 1]$.

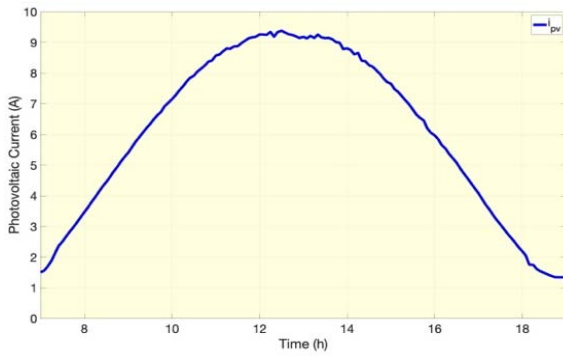


Fig. 5. Photovoltaic current $i_{PV}(t)$.

Then, the optimization problem (6) considering LMI conditions (17), (18) and (19) has been solved using the MATLAB's *mincx* function, the SCILAB's *lmisolver* function and the PYTHON's *cvxopt* function for the three fault sensor cases and for $\alpha = -1, -10$ and -100 (transient performance), $\zeta = 1$ (disturbance rejection) and $\mu_1 = \mu_2 = 1000$ (limitation of gain values). Table 3 show the robustness bound values obtained for each case, respectively for α . In order to facilitate the reading of these results, the values of the robustness bounds appearing in the table are multiplied by 100. Each robustness bound represents the fault tolerance of the remaining sensor affected, S_{i_L} , S_{v_o} or $S_{v_{pv}}$. Colored cells correspond to the highest bound.

Generally, MATLAB seems to give significantly better results for $\alpha = -1$ and $\alpha = -10$ except for case 3 where the best fault tolerance is obtained with PYTHON. It is logical to obtain less robust control laws for $\alpha = -100$, however it should be noted that

SCILAB is the most efficient in this case. In order to compare the quality of these FTC control laws, we carried out a simulation with Simulink for case 3 (fault on $S_{v_{pv}}$ sensor) and $\alpha = -10$. The magnitude of the considered fault is the one corresponding to the largest robustness bound, $\rho^{*Py} = 0.00686$, obtained with PYTHON. For information, we give the gains of the controllers obtained by the three solvers and associated with the control law given in Table 4.

$$\begin{cases} u(t) = 0.5 + \delta u(t) \\ \delta u(t) = k_i e(t) + k_{p1} i_L(t) + k_{p2} v_o(t) + k_{p3} v_{PV}(t) \end{cases} \quad (20)$$

Table 3. Robustness bounds $\rho^* \cdot 10^2$.

Case	α	LANGUAGE		
		MATLAB	SCILAB	PYTHON
1	-1	1.0836	0.9971	0.9474
	-10	0.4582	0.3824	0.4113
	-100	0.720	0.1346	0.0995
2	-1	0.8935	0.8396	0.75783
	-10	0.7364	0.6713	0.7003
	-100	--	--	--
3	-1	0.4578	0.4198	0.3901
	-10	0.6348	0.5768	0.6860
	-100	0.0848	0.0490	0.0320

Table 4. Gains obtained with the three solvers.

SOLVER	Gain			
	k_i	k_{p1}	k_{p2}	k_{p3}
MATLAB	-28.3943	-0.1921	0.0136	0.1831
SCILAB	-60.5522	-3.2052	0.1301	3.0070
PYTHON	-1644.892	-5.1347	0.4208	4.3108

For simulation purposes, the fault is associated with an additive uncertainty on the output matrix, such as:

$$C(\Delta) = \mathbb{I}_3 + \begin{bmatrix} 0 \\ 0 \\ 1 \end{bmatrix} \cdot \rho^{*Py} \cdot \sin(2 \cdot \pi \cdot t) \cdot [0 \ 0 \ 1] \quad (21)$$

Photovoltaic voltage $v_{PV}^*(t)$ respectively obtained with MATLAB, PYTHON and SCILAB are compared with $v_{PVref}(t)$ in Fig. 6. The three control laws are rather fault resilient but it is clear that the voltage regulation is better with the state feedback matrix K

generated by PYTHON. This is highlighted by the Fig. 7 which presents a zoom of Fig. 6. Finally, Fig. 8 shows the shape of the control inputs associated with the three previous control laws. Note that the signal generated by the controller respects $0 \leq u(t) \leq 1$.

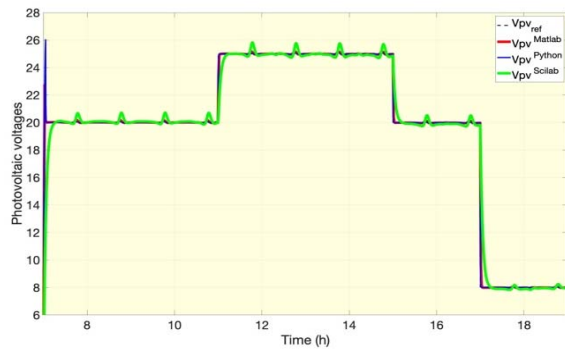


Fig. 6. Regulated photovoltaic voltages $v_{PV}^*(t)$.

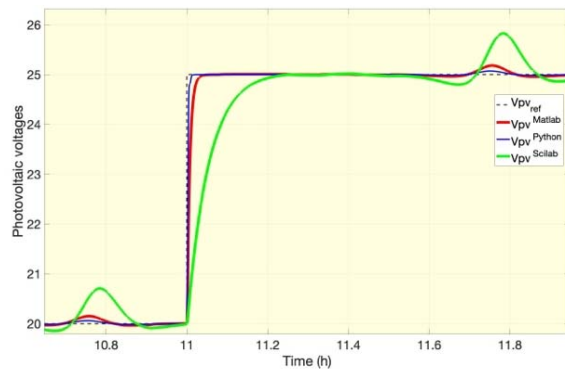


Fig. 7. Zoom of regulated photovoltaic voltages $v_{PV}^*(t)$.

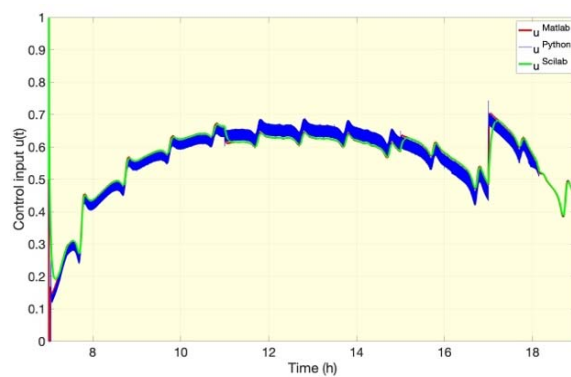


Fig. 8. Control signal $u(t)$.

5. Experimental Tests

The effectiveness of the proposed FTC control approach is approved by experimental tests on an experimental platform. This stand-alone test bench, illustrated in Fig. 9, consists of a photovoltaic chalet equipped, on its roof, with 30 photovoltaic panels with a power of 233Wc and monocrystalline technology.



Fig. 9. SMART-EnR platform: photovoltaic chalet.

The experimental setup, located inside the chalet and shown in Fig. 10 had been implemented with the following equipment:

- ① PV panel
- ② Li-ion batteries
- ③ Acquisition of solar irradiance and temperature measurements
- ④ MicroLabBox-dSPACE card
- ⑤ DC-DC boost converter
- ⑥ Two bidirectional converters built using SEMIKRON power modules
- ⑦ Voltage and current sensors
- ⑧ The graphical user interface on *ControlDesk* software.

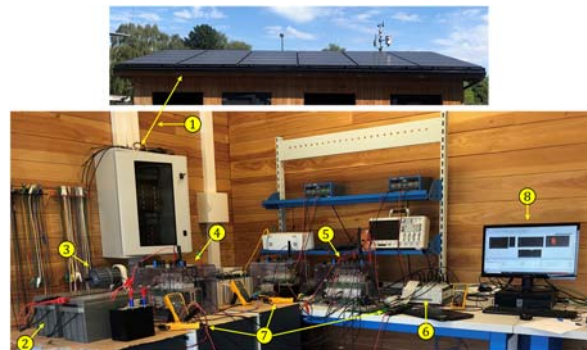


Fig. 9. Experimental test bench of PV/battery system.

This test was performed on April 11, 2023 at 11:17 a.m. over a period of 650 seconds. Weather conditions during this period are relatively stable with an ambient temperature of around 15 °C and solar irradiance shown in Fig. 10.

Only one of the 30 photovoltaic panels is connected to the Li-ion batteries. The DC-DC boost converter is the same as the one described section 3 and the control law implemented is the one given in (20) with the coefficients of the PYTHON solver appearing in Table 4. We simulated a fault sensor fault of the photovoltaic voltage by multiplying the value of $v_{pv}(t)$ by $(1 - \rho^{*Py})$ between 11:21:46 a.m. and 11:22:26 a.m. The sensor fault period is illustrated by

the blue area in Fig. 10. This fault has the consequence of disturbing the MPPT algorithm which exploits the measurement of $v_{pv}(t)$ to generate $v_{pvref}(t)$.

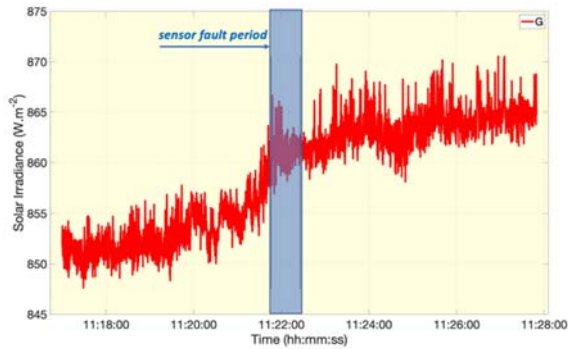


Fig. 10. Solar irradiance and sensor fault period.

Despite this sensor defect, Fig. 11 shows that the regulation of the photovoltaic voltage is excellent. This observation is definitively validated by Fig. 12 which is a zoom of Fig. 11 during the sensor fault period. It is important to remember that the performance of this reference voltage tracking is closely linked to the choice of the half-plane C^α . The more the half-plane is offset from the imaginary axis of the complex plane, the better the performance of the controller in terms of response time. For this experimental validation, $\alpha = -10$.

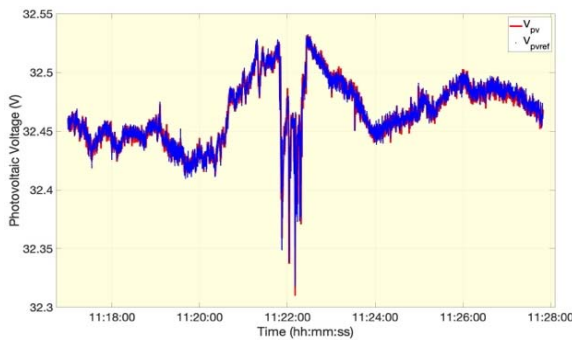


Fig. 11. Tracking of $v_{pvref}(t)$.

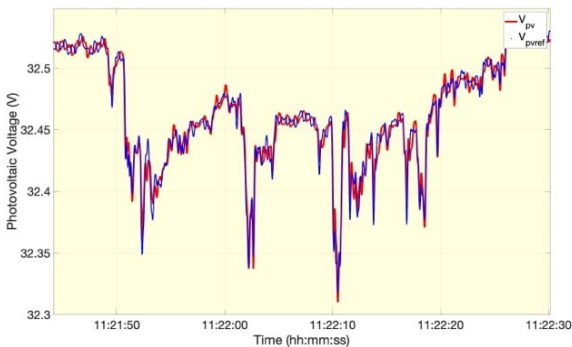


Fig. 12. Zoom of Fig. 11 during sensor fault period.

Finally, the duty cycle generated by the controller and the photovoltaic power produced by the PV panel are respectively illustrated in Fig. 13 and Fig. 14. The switching frequency of the MOSFET thyristor is 20 kHz. We can see that the value of the duty cycle is almost constant during this test despite a more significant variation around 11:22:00 when we simulated the sensor fault.

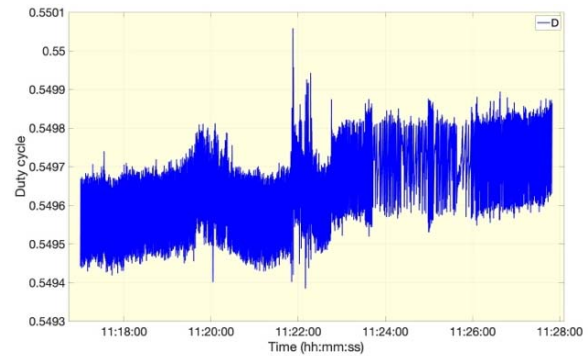


Fig. 13. Duty cycle (D).

Fig. 14 shows a slight decrease in the photovoltaic power produced by the panel during the sensor fault. This decrease is not due to a lack of performance of the controller which allows a very good tracking of $v_{pvref}(t)$ but at a bad value of this reference, computed by the MPPT algorithm and falsified by the fault.

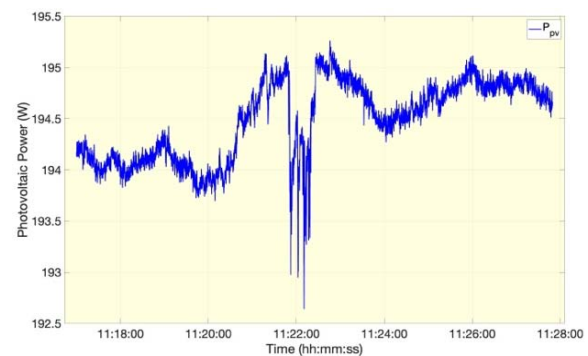


Fig. 14. Photovoltaic power (P_{pv}).

6. Conclusions

This paper deals with fault resilience of DC-DC boost converter sensors associated with a robustness bound generated by a state feedback control technique. The resulting problem was solved using three LMI solvers provided by different programming languages. The contribution of this study is not to the development of a new fault-tolerant control technique but rather to the robustness analysis (and therefore the fault resilience) associated with a control law,

depending on solver. The results presented in sections 4 and 5 show that the robustness of the control laws can be influenced by the solver used. However, it is not possible to conclude as to the most efficient solver because it depends on the case study. The simulation results but also the experimental tests validate the fault-tolerant control technique considered in this work. This state feedback control technique can only be effective when the fault is partial. If the fault is complete, the output feedback case should be considered and this constitutes an interesting perspective for this work.

References

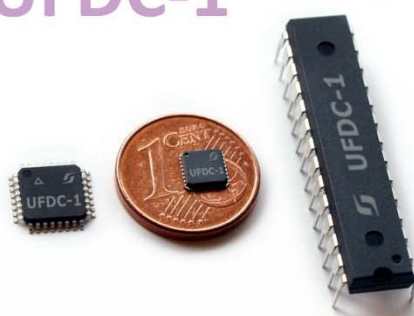
- [1]. C. V. Lozano and K. K. Vijayan, Literature review on Cyber Physical Systems design, *Procedia Manufacturing*, Vol. 45, 2020, pp. 295-300.
- [2]. A. Baldini et al., Fault Tolerant Control for remotely operated vehicles with thruster faults using non linear disturbance observers, *IFAC PapersOnLine*, Vol. 55, Issue 31, 2022, pp. 275-280.
- [3]. Y. Zhang et al., Fault Diagnosis and Fault Tolerant Control of energy maximization for wave energy converters, *IEEE Transactions on Sustainable Energy*, Vol. 13, Issue 3, 2022, pp. 1771-1778.
- [4]. A. B. Masood et al., Control over blockchain for Data-Driven Fault Tolerant Control in Industry 4.0, in *Proceedings of the IEEE Mediterranean Communication and Computer Networking Conference (MedComNet)*, Pafos, Cyprus, 01-02 June 2022, pp. 131 - 139.
- [5]. M. A. Ragaieg et al., A robust output feedback input constrained design for a class of LPV system, in *Proceedings of the Mediterranean Conference on Control and Automation (MED'2020)*, Saint-Raphaël, France, September 2020, pp. 284 - 291.
- [6]. A. Cherifi et al., Global non-quadratic D-stabilization of Takagi-Sugeno systems with piecewise continuous membership functions, *Applied Mathematics and Computation*, Vol. 351, Issue 1, 2019, pp. 23-36.
- [7]. G. Chesi, LMI conditions for time-varying uncertain systems can be non-conservative, *Automatica*, Vol. 47, Issue 3, 2011, pp. 621-624.
- [8]. X. Fan et al., A fuzzy Lyapunov function method to stability analysis of fractional-order T-S fuzzy systems, *IEEE Transactions on Fuzzy Systems*, Vol. 30, Issue 7, 2022, pp. 2769-2777.
- [9]. F. Y. Nesterov and A. Nemirovskii, Interior-point polynomial algorithms in convex programming, *SIAM*, 1994.
- [10]. J. Yuan and A. Lamperski, A random algorithm for semidefinite programming problems, in *Proceedings of the American Control Conference (ACC' 2018)*, Milwaukee, USA, June 2018, pp. 1382 - 1387.
- [11]. S. Sra, S. Nowozin and S. J. Wright, Optimization for machine learning, Neural Information Processing series, *The MIT Press*, September 2011.
- [12]. B. O'Donoghue et al., Conic optimization via operator splitting and homogeneous self-dual embedding, *Journal of Optimization Theory and Applications*, Vol. 169, No. 3, 2016, pp. 1042-1068.
- [13]. R. Nikoukhah, F. Delebecque and L. El Ghaoui, LMITOOL: a package for LMI optimization in Scilab User's guide, *Research Report RT-0170*, inria-0007000, 1995.
- [14]. S. Boyd, L. El Ghaoui, E. Feron and V. Balakrishnan, Linear Matrix Inequalities in system and control theory, *SIAM*, 1994.
- [15]. F. N. Lagunes et al., Impact of the programming language used to solve a LMI problem on the fault resilience of cyber-physical systems, in *Proceedings of the 3rd IFSA Winter Conference on Automation, Robotics & Communications for Industry 4.0/5.0 (ARCI' 2023)*, Chamonix, France, February 2023, pp. 49-53.




Published by International Frequency Sensor Association (IFSA) Publishing, S. L., 2023
(<http://www.sensorsportal.com>).

Universal Frequency-to-Digital Converter (UFDC-1)

UFDC-1



- 16 measuring modes: frequency, period, its difference and ratio, duty-cycle, duty-off factor, time interval, pulse width and space, phase shift, events counting, rotational speed
- 2 channels
- Programmable accuracy up to 0.001%
- Wide frequency range: 0.05 Hz ... 7.5 MHz (120 MHz with prescaling)
- Non-redundant conversion time
- RS232, SPI and I²C interfaces
- Operating temperature range -40 °C ... +85 °C



<https://www.sensorsportal.com/>
info@sensorsportal.com